Research article

Experimental investigation of the parameters that affect droplet size and distribution for design calculations of two-phase separators

Kul Pun [a,*], Faik Hamad [a], Tariq Ahmed [a], Johnson Ugwu [a], Safa Najim [b], James Eyers [c], Gary Lawson [c], Paul Russell [a]

[a] *School of Computing, Engineering & Digital Technologies, Teesside University, Middlesbrough, Tees Valley, TS1 3BX, UK*
[b] *Electrical Engineering Department, College of Engineering, Basrah University, Basrah Iraq*
[c] *DarbyTech Engineering, 17 Evolution, Wynyard Park, Billingham, TS22 5TB, UK*

ABSTRACT

The critical design parameter when sizing a separator is the size of oil droplets in the water phase. This study improves the design of a separator by investigating the parameters that control droplet size, frequency, and distribution.

Experimental work was performed to investigate the effect of flow rates and oil layer thickness on these parameters. Experiments were performed using a transparent laboratory separator to allow the measurement of droplet properties. The Design of the Experiment (DOE) method with the Taguchi analysis was applied to investigate statistically if droplet properties are solely a function of the independent variables or if they interact.

The findings show that the results can be modelled using Gaussian distributions. Droplet size distribution and the number of droplets produced are functions of the interaction between oil flow rate and oil pad thickness. The oil flow rate dominates the droplet size though layer thickness has a minor effect. The number of droplets (Frequency) increases with both oil and water flow rates but decreases with oil pad thickness. There are clear interactions between all variables resulting in different droplet frequencies for combined effects. The distribution of the droplet sizes is controlled by oil layer thickness, where the spread is seen to rise with thickness. However, interactions between the fluid flows and oil pad thickness give rise to different droplet distributions if either variable were changed on its own.

1. Introduction

The current global position on climate change is to reduce fossil fuel usage to reduce carbon emissions at COP26 [1]. However, there is a dichotomy in that the crude oil and natural gas industries have experienced rapid growth in recent years. The global demand for crude oil and liquid fuels averages 100.6 million b/d for 2022, up 3.1 million b/d from 2021, increasing by 1.9 million b/d in 2023 to average 102.6 million b/d, according to the U.S. Energy Information Administration's [2] Production companies have increased production to meet this demand. Equally, the operational reservoirs are depleted, and enhanced techniques are required to improve

---

recovery efficiency; therefore, the production equipment must be replaced.

The multiphase separator is the key piece of topside upstream production equipment used by the oil and gas production system. The oil and gas industry will spend USD 8.9 billion on three-phase separators in 2022 [3]. Therefore, the case is made that it is essential to improve the design of this piece of process equipment. If this design is to be improved, it is essential to understand the theory behind its operation.

How does a two-phase separator work?

These separators come in various shapes and sizes, but their primary goal is the same, separation of the phases by gravity. The initial portion near the inlet (see Fig. 1) is where turbulent mixing occurs. The inflow of oil and water hits the inlet diverter plates, mixes with the continuous water phase at the bottom of the vessel and rises through the oil-water interface. During this stage, coalescence of the oil phase takes place, forming droplets.

The second flow regime (see Fig. 2) Occurs further down the separator, where the flow becomes laminar, and gravity settling of the droplets occurs. An oil pad is formed on top of the water layer. In the oil-continuous phase (oil pad), water droplets fall perpendicular to the bulk flow. In the water-continuous phase, oil droplets rise from the bottom of the tank to the oil-water interface. The separation time for the settler is determined by the settling time for a droplet of water from the top of the oil layer to the oil-water interface or the rise time for a droplet of oil from the bottom of the settler to the oil-water interface. The longer time is the controlling factor, but ideally, these should be balanced.

The settling times for each layer are dependent on several factors, including but not limited to: the thicknesses of the oil and water layers; the diameter, volume, size distribution, and the number of droplets; the physical properties of the fluids themselves, including density, viscosity and surface tensions. Therefore, the solution to the settling times is complex.

The settling time for water from the oil phase is given in equation 1

$$T_s = \frac{\text{oil pad thickness}}{\text{settling velocity}} \tag{1}$$

Where settling velocity is determined from a force balance upon the droplet (See Fig. 3)

A relative motion exists between the droplet and continuous phase when separating oil droplets from water or water droplets from oil. A density gradient between the continuous and dispersed phases is present; dispersed droplets experience an upward force due to buoyancy and a downward force due to gravity. A third force due to the continuous phase (water) imposes a drag force F_D which opposes the direction of motion. The balance between these forces results in a constant velocity for the droplet. Therefore, oil droplets continue to rise at a constant velocity known as settling velocity (u_t). The gravitational effect accounting for buoyancy is shown in equation (2).

$$F_G = (\rho_w - \rho_o)\frac{\pi}{6}D^3 \tag{2}$$

The drag force is accounted for by Stokes law equation (3).

$$F_D = C_D\frac{\pi}{4}D^2 * \frac{\rho u_t^2}{2g} \tag{3}$$

Where the drag coefficient from the right-hand side is given as

$$C_D = \frac{24}{R_e} = \frac{24 * \mu * g}{\rho D u_t} \tag{4}$$

Substituting for C_D from equation (4) into equation 3

$$F_D = 3\,\pi\mu\,Du_t \tag{5}$$

The settling velocity is reached when the drag force (F_D) is equal to gravitational force (F_G) Substituting equation 3 into 5 to find the droplet settling velocity using equation (6).
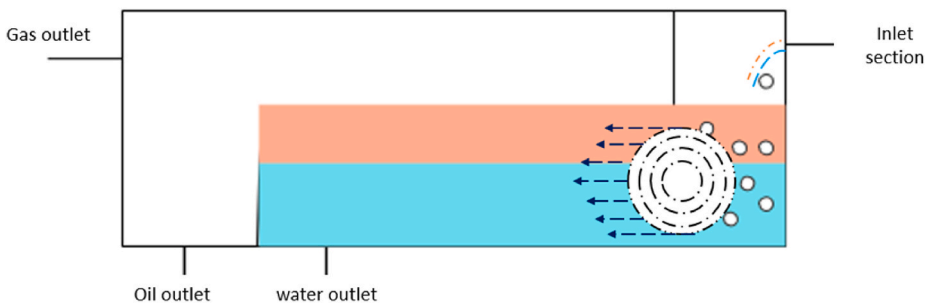

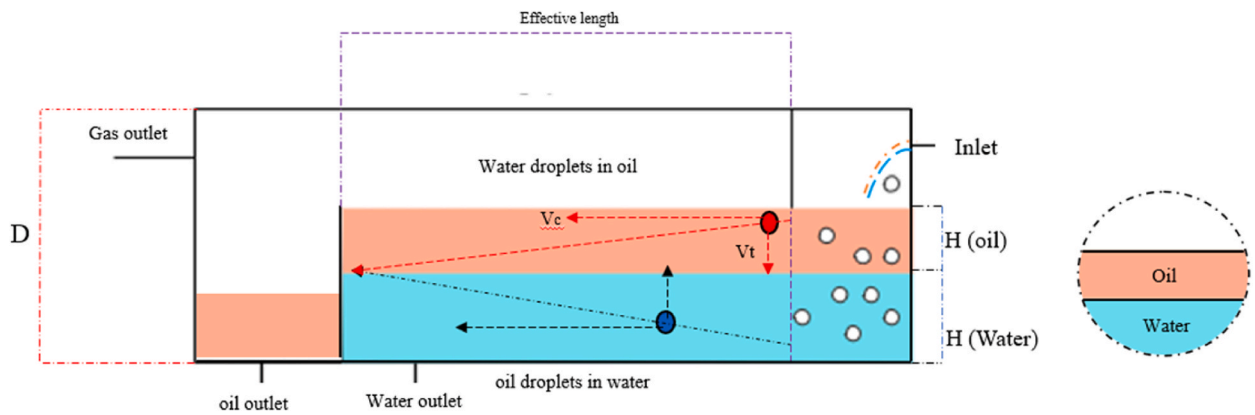**Fig. 1.** Illustration of coalescence and separation of oil droplets.

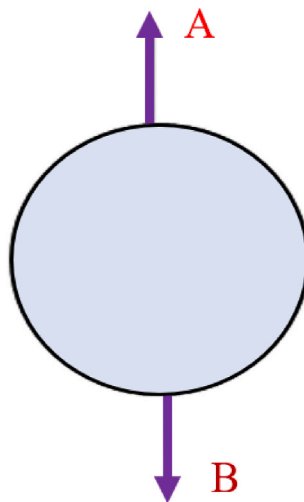**Fig. 2.** Settling movement of oil and water droplets.

Fig. 3. Forces acting on the oil droplet during separation (A) drag force, (B) gravity force including buoyancy force.

$$u_t = \frac{(\rho_w - \rho_o) * D^2}{18 * \mu}$$

(6)

Where D is the particle diameter, g is the acceleration caused by gravity, ρ_w is the density of water, ρ_o is the density of oil, u_t is the setting velocity, μ is the viscosity of fluid, F_D gravitational force due to drag, C_D Drag coefficient.

1.1. What factors related to droplet size are critical to the separation process?

1.1.1. Droplet diameter
From equation (6), all variables are known fluid properties apart from droplet diameter. The importance of the settling time of droplet diameter is compounded by the fact that the velocity varies as a square of the diameter. Therefore, accurate knowledge of the droplet size is essential to determine the settling time and, thus, the separation achieved. Factors affecting the droplet size within the separator are also critical to achieving separation.

1.1.2. Layer thickness
The layer thickness is defined as the depth of the oil layer on top of the water layer from the separator inlet head to the Weir [4]. states that the oil pad layer is one of the main factors in controlling droplet settling and separation.

1.1.3. Flow rates
Flow rates are known factors that directly impact droplet size; as the flow rates increase, the fluid's momentum increases shear forces, resulting in smaller droplets. Equally, the smaller the droplet, the slower it settles, and its tendency to coalesce into bigger drops is reduced. Therefore, it is essential to determine how a change in flow rate affects the separation process.

1.1.4. Droplet size distribution

Previous research in this area [4] identified a problem with current design methodologies, including [5,6] models. They assumed a single nominal droplet size when setting the design calculations of 500 μm, which leads to conservative equipment design. In practice, a fluid mixture is not just a single uniform droplet size dispersed in a continuous medium but a droplet size distribution. The droplet size distribution determines the fraction of recoverable oil, as any droplets smaller than the set droplet diameter used for design will not be recovered. The shape of the distribution (see Fig. 4a and b) will affect the fraction of droplets recovered and, in its simplest form, depends upon the peak droplet size (see Fig. 4b) and spread of the peak (see Fig. 4a).

As a result, a systematic investigation of the effect of droplet size and the relevant parameters discussed in section 1.1 on separation is required.

2. Literature survey of concerning droplet size

On investigation of the extant literature, droplet size is a major issue with design models [7]. stated that "droplet diameter has been the primary cause of the gap between experimental and CFD results" As a result, several researchers [4,6,8–11], and [12] made assumptions about droplet size distributions for their design methods without investing effort to try to close this gap.

2.1. Experimental measurements of droplet size for three-phase separators

[13] suggested that experimental investigation is not viable. Because of the high-performance cost and technological issues in monitoring the internal flow behaviour of oil and water within an industrial separator.

The only known experimental work for three-phase separators is described below [14]. Proposed a method for sizing three-phase separators using a droplet size distribution. They tested their method using a three-phase separator with a diameter of 4420 mm and an overall length of 15850 mm and the Sauders-Brown equation with an appropriate k factor for gas-liquid separation and an actual retention time obtained from lab and field experiments to find the liquid-liquid separation.

The results confirmed that oil droplets greater than 91 μm and water droplets greater than 89 μm would separate from the gas. The oil droplets smaller than 60 μm would be lost in the water outlet of the three-phase separator. The maximum droplet size of water carried over with the oil stream is 225 μm and would be lost in the oil outlet resulting in a 4.5% separation efficiency.

2.2. Numerical simulations for droplet size distributions

The complicated mathematics and long calculation times involved in simulating three-phase flows have led to most studies focusing on the more straightforward case of two-phase separators, with only a few studies dealing with three-phases.

[4] used VOF and Eulerian models included in the ANSYS Fluent simulation package to simulate a three-phase separator with a diameter of 300 mm and a length of 900 mm [4]. also incorporated the k-ε model to simulate turbulent flow. For fixed flows of 2 and 10 GPM for both oil and water phases, they modified their model by changing the mean droplet diameter used from the normal 500 μm [4] to see if they could improve the agreement between simulation and experimental results. Note They did not measure the droplet size distribution for the experiments preferring to infer it from the model fits. They used the following six droplet diameters 100, 200,350, 500,750 and 1000 μm. They found that the low flow of 2 GPM CFD predictions using 500 μm underestimated the experimental results by 10% for separation in the oil phase. Changing the droplet size did not affect the agreement. However, at 10 GPM, where it would be expected that the droplets have reduced in size, they found that the CFD overestimated the separation by 15% for 500 μm particles. When they reduced the diameter to 350 μm, they improved agreement to 1.5%. They concluded that the model is very dependent on mean droplet size, and some way needs to be found to link flow rate to droplet size to improve design simulations.

[15] **used several types of** vessel configurations based on the fluid properties of an Iranian three-phase separator. The computational fluid dynamic (CFD) method for analysing the three-phase separation combined with the volume of fluid–discrete particle
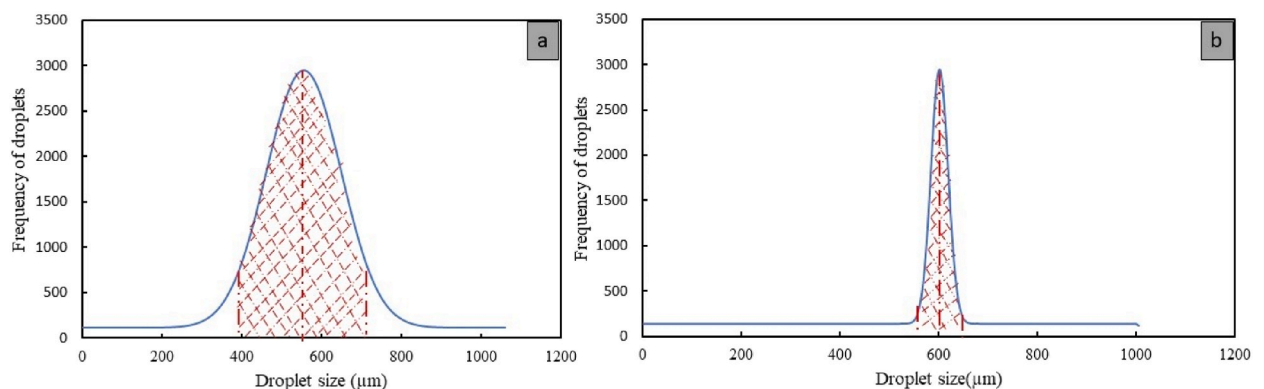

Fig. 4. The shape of bubble distribution (a) spread distribution (b) spread of the peak distribution.
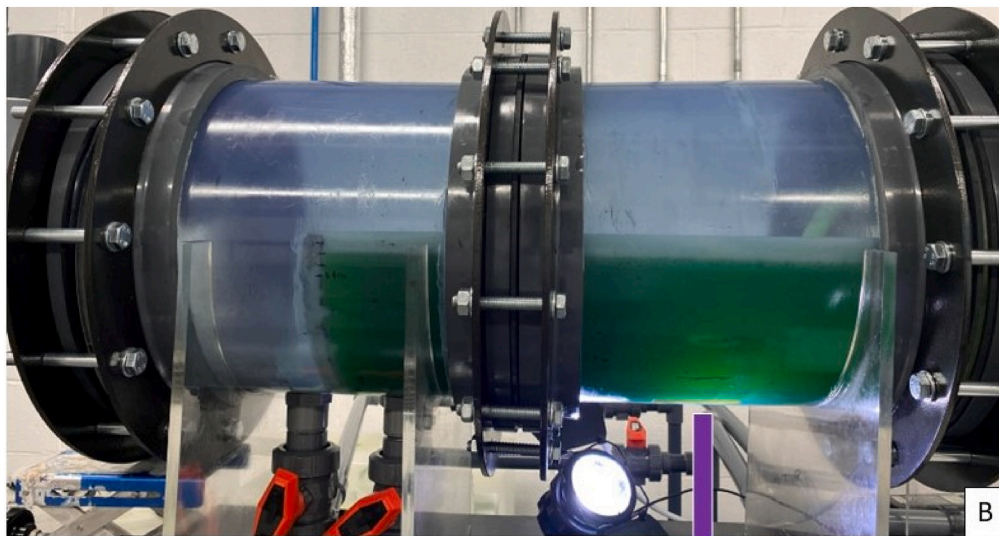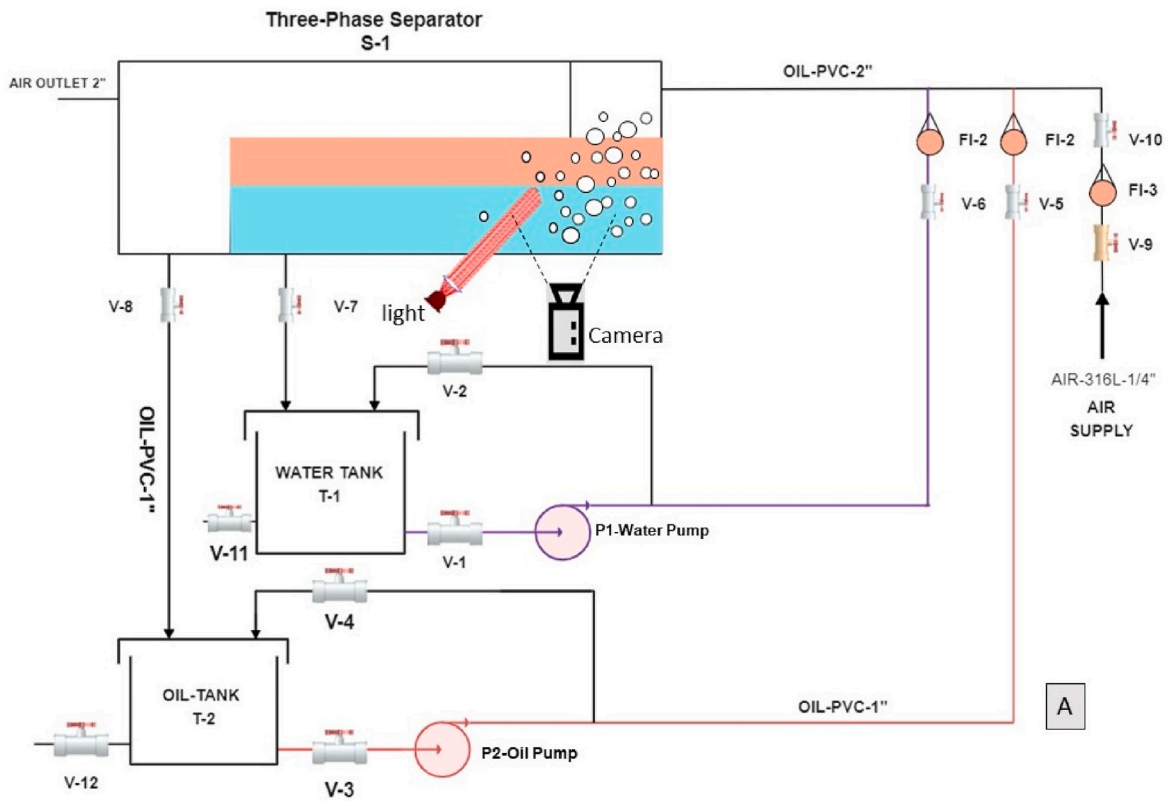
Fig. 5. (A) Schematic diagram of the experiment setup and (B) Photo of the test rig highlighting the area of droplets captured at Teesside university.

method (DPM) and three different turbulence models, i.e., standard k–ε, standard k–ω and RSM, studied with the droplet diameters of 1250, 1550,1850 2150 and 2500 mm. The simulation results show that the droplet coalescence occurred at less than 0.5% in 3, 6, and 7 cases. For these cases (3,6, and 7), the droplet break-up occurred at 15.10%, 17.94%, and 18.375%, respectively. As a result, the efficiency of the case (3) vessels was improved due to the installation of a vane-type inlet plate.

[12,16] used (CFD) an Eulerian-Eulerian multiphase, to predict separation efficiency and a population balance model to predict the evolving droplet size distribution of the pilot-scale high-pressure three-phase separator with a length of 3000 mm and a diameter of 700 mm. In this case, the droplet distribution is produced artificially using a perforated plate and is not solely a function of the inlet flow. A perforated plate produces the evolution of the droplet sizes distribution mounted 750 mm from the inlet flange. Sentech profilers are mounted downstream of the water outlet and upstream of the Weir to measure the droplet distribution (2250 mm from the inlet flange). They observed that the droplet diameter increases with retention time and water fraction. The droplet sizes are smaller at a high flow rate, have a higher turbulent mixing level, and produce smaller droplets with less retention for droplet coalescence. The coalescence rate is not fast enough to grow the droplets to a larger diameter than in the lower flow rate cases. The larger droplets settle to the interface quickly, resulting in a larger droplet diameter above the interface.

Aside from this, many CFD studies have been performed to find droplet diameter distributions, but the literature review revealed that little or no work had been done to confirm their distributions with actual separator bubble distribution data. Therefore, the case is proven for an experimental study to look at closing the gap in knowledge about droplet size and distribution for separators for real experimental data.

3. Experimental setups

A variable geometry experimental apparatus was developed at Teesside University to investigate the effect of the L/D ratio on separator performance by Ref. [4]. This apparatus has been modified to allow the measurement of droplet size.

3.1. Overview of the experimental test-rig

The Teesside University horizontal three-phase separator (HTPS) is made from transparent polypropylene, allowing visual observation of the separator's flow regimes. It has a fixed diameter of 300 mm and a length range of 600 mm–1500 mm, giving an adjustable L/D ratio of 2:1 to 7:1. The length is modified by adding a mix of pipe sections of 300 mm and 600 mm.

Fig. 5 (A) show the Piping and Instrument Diagram (P&ID) and the experimental rig setup photo Fig. 5B.

The separator is equipped with two Clarke SPE800 pumps with a power capacity of 800 Watts with a 230V motor, each capable of pumping 53 l/min of liquid with a maximum head of 40 m. Potable water was used for the heavy liquid, and Shell Tellus industrial hydraulic fluid was used for the light liquid. The water was coloured Green using food dye to increase the contrast between oil and water and identify the interface. The physical properties of the water-oil phase density are 1000 kg/m^3 and 800 kg/m^3, respectively.

The apparatus has been modified to measure the droplet distribution. Measurements are made in the separator body, not the inlet pipe because the inlet geometry can change the droplet size distribution. The apparatus has been fitted with light below the inlet deflector. A camera is mounted at right angles to the separator to capture the oil droplets rising through the water layer.

3.2. Experimental methods and procedures

This experimental programme aimed to determine the droplet size distribution for a given set of flow measurements. Experiments were confined to droplet sizing, and no measurements were made as to the separator's performance. A typical experiment would start with an empty separator, all valves shut, and the pumps switched off. Return valves in the kickback lines are opened halfway, as are the discharge valves V5 and V6. The pump inlet valves are then opened to allow fluid to move into the pumps and prime them under the static head from the feed tanks. The pumps are then started, and the kickback valves and discharge valves are adjusted to give the desired flow rates. Usually, the system is set to operate at the lowest measurable flow. The liquid level rises slowly in the separator and establishes an oil pad on top of the water layer. The water liquid level is controlled by adjusting the ball valve V-7. During operation, this was utilised to change the height of the oil-water interface. The oil builds up and overflows on a fixed height weir set to run at the centreline of the separator. Adjusting ball valve V-8 controls the outlet flow rate of oil from the 1-inch pipe downstream of the Weir. The apparatus is run for 15 min at a steady state to establish the initial steady-state concentrations of the phase. Once a steady state was established, photographs of the droplet distribution were taken. A video of the droplet flow was recorded simultaneously to consider the dynamic droplet behaviour if problems were encountered when analysing the still data. Experiments were carried out in a random pattern to avoid establishing hysteresis.

Finally, the oil flow stops, the pump shuts down, and the oil-water interface rises until the interface reaches the top of the Weir. The water valve V-8 is then opened fully, and the water pump is shut down, allowing the water to drain back into its feed tank. Water entrained in the oil outlet can settle in T-2 and be removed from V-12. Oil entrained in water is skimmed from tank T-1 and returned to the oil tank.

3.3. Image capture measurement

3.3.1. Introduction

The comments of [13] about the prohibitive cost of size distribution measurements in commercial apparatus made it important to

find a cheap, robust, and straightforward technique to measure droplet size and distribution. Still, photography with image processing offered a straightforward way to achieve this. Several authors [17,18] have used these techniques to find multiphase flow's bubble/droplet diameters. The authors also have experience with this technique from previous microbubble projects [19].

It was decided to measure the droplet size distribution in the main separator body just after the fluid enters the separator rather than the inlet pipe (see figure no 5). This position gives the actual droplet distribution in the separator. It also takes account of any droplet coalescence as the inlet flow passes through the oil layer. It is easier to measure than the inlet pipe because the droplets are spread out and moving less quickly.

3.3.2. Experimental method used to determine droplet size

After the steady state was established, the droplet distribution of oil and water was captured using a SONY Alpha 7 (III) camera with a 28–70 mm Zoom Lens by observing the rising motions of bubbles at the viewing section the separator inlet and capturing them as still images. The fluid was illuminated using a 100 W LED studio lite panel light mounted perpendicular to the camera. The parameters of the high-speed camera were set as follows: resolution 1920 × 1080, frame rate 500 f/s and record-setting of 50P 50 M, which provided the largest viewing area. For better visualisation, the camera has been accurately aligned horizontally and located 100 mm from the test rig. To reduce errors, working distance, focal length, and field depth were fixed and checked in every experiment.

The oil-water's two-phase recorded images were stored in a personal computer and processed using image analysis software. The recorded frames were examined and selected carefully. The camera images were calibrated to convert the still image captured as pixels into actual metric dimensions [20]. A single drop of known dimensions was photographed under the same conditions as the actual measurement and used to obtain a relationship between pixels and mm. Each image was magnified by a factor of five to give the desired resolution. Each pixel was found to represent an actual distance of 53 μm. The work of [14] stated that droplets less than 60 μm would be lost in the water phase anyway. Thus, this represents an acceptable accuracy of detection for the droplets of interest.

3.3.3. Calibration of droplet size measurement technique

To test the accuracy and reproducibility of the measurements made it was decided to carry out some test measurements on sample glass ballotine (see Fig. 6A) and alumina oxide pellets (see Fig. 6B) of known size. The pellets used were known to vary in size within a specific size range; therefore, it was decided to take a sample of each type of pellet and measure its dimensions in different positions. Six ballotine beads and six alumina oxide pellets were measured using a digital calliper accurate to 10 μm.

Each pellet was then dropped into a glass tube containing a mix of oil and water dyed to the same colour as that used in the separator. Sample photos for each type of pellet falling in water are shown in (Fig. 6A and B). The fall of each pellet was recorded using the same camera setup as that for the separator experiments, and the film was processed in the same way (See section 3.4)

The results of these experiments are recorded in table (1)

The results show the image J software measurements repeatedly agree to better than 1% or 10 μm (the limit of accuracy of the calliper) with the calliper measurements. This accuracy is acceptable for the measurements made on the separator where the smallest sizes recorded is greater than 60 μm.
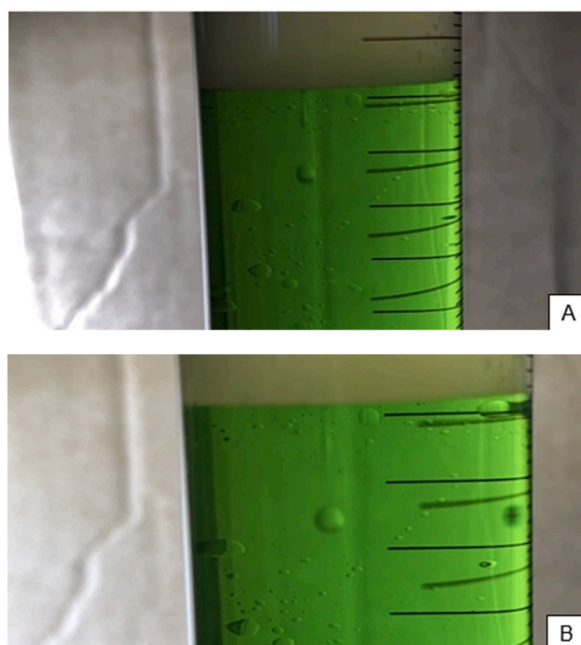

Fig. 6. Photo (A) shows a falling ballotine in water. Photo (B) shows a falling alumina oxide pellet in water.

3.4. Image analysis processing

The next step was to develop a standard method to analyse the photographs and the derived droplet data. This is described below:

The bubble diameter distributions captured by the camera were extracted using an image analysis tool (Image J). Image J is a freeware java-based image processing programme faster and more accurate than sieve analysis [21]. This tool has been used in various applications, including biomedical, powder technology, and food processing, and can evaluate various size and shape criteria [21]. The steps involved in image procession are shown schematically in Fig. 7.

Step 1. involves taking the camera's colour image and converting it to an 8-bit grayscale image. A single grayscale image of the typical photograph image produced for a system is presented in Fig. 7. If the image is over-illuminated, the lighting is adjusted by subtracting the background lighting level [22]. The threshold value for the normalised image is then applied in step 2. The contours now highlighted correctly approximate real-world interface locations because maximum grey level intensity gradients may be determined. Step 3 converts the image into a pure binary black-and-white image. This conversion is achieved by applying a global threshold. Binarised processing contains several processes to minimise image noise while maintaining the structure of binary objects: area opening, median filtering, thinning, thickening, picture filling, and skeletonisation [19,23]. In step 4, the image of the round item was detected using the circular Hough transform [24]. The circular object bubbles were then extracted using the multi-edge detection approach [25]. The next step uses the calibration data from the measured single droplet to scale the image. The software then converts the extracted bubbles into sized images and counts the droplets in given ranges (see Fig. 8).

3.4.1. Post-image processing of the numerical droplet distributions

After image processing, the image software produces an output that lists droplet counts and their specific areas (μm^2). These were then processed in Microsoft excel software to determine the radius and diameter of the droplet in each category in μm. The list of diameter categories is over 20,000, which is too large to analyse sensibly, but many of the categories are repeated. Therefore, the categories with common diameters were added to give the total count of droplets with a given diameter.

This data is shown as a plot of the mean bubble diameter versus the number of bubble droplets in Fig. 9.

3.4.2. Fitting model with Gaussian curve

A first examination of the droplet diameter versus droplet frequency plots (Fig. 9) suggested that a bell-shaped curve could fit the data. Given their relative simplicity, Gaussian distributions were chosen to fit the data,

The Gaussian distribution equation (7) is shown below

$$y = y_0 + Ae^{-\frac{(x-x_c)^2}{2w^2}} \qquad (7)$$

Where,

y_0 = Baseline offset, .
A = amplitude total number of particles, .
x_C = centre of the peak.
w = FWHM full width of the peak at half height.

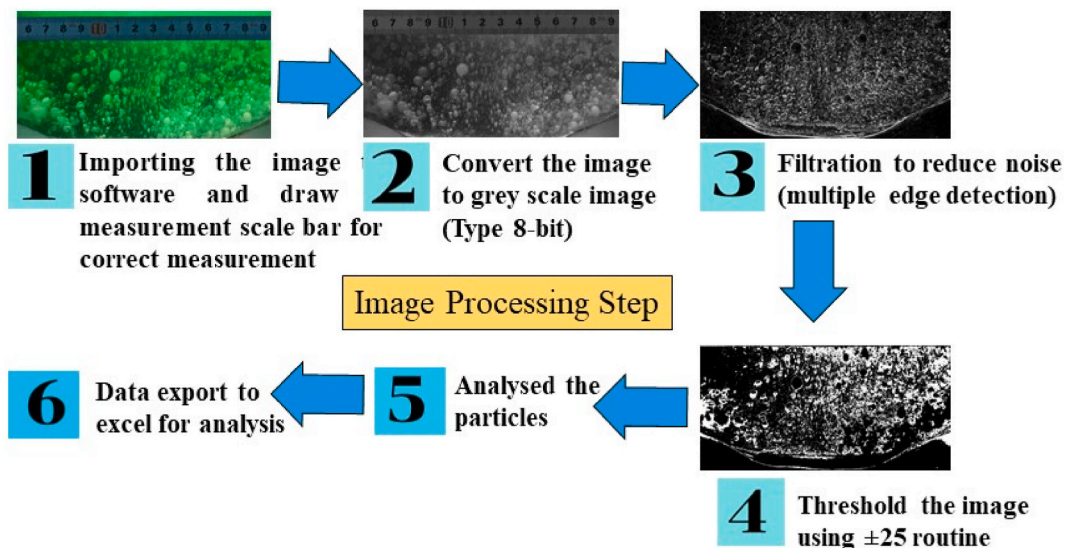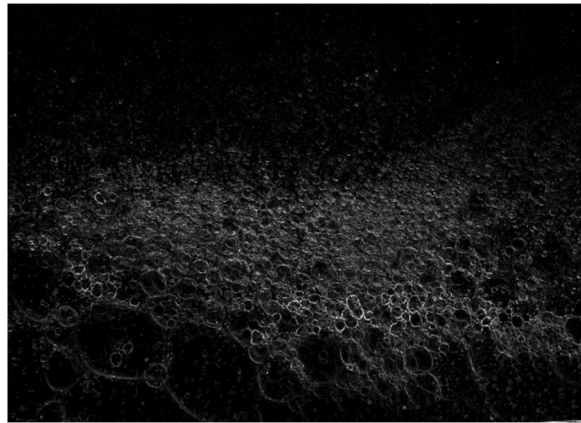**Fig. 7.** Flow diagram steps of calculating droplet size using image j.

Fig. 8. Photographic image produced from image j at oil and water flow setting at 1.589 m^3/h.
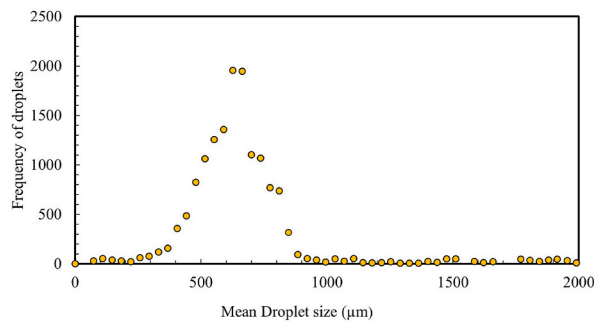

Fig. 9. Experimental Result of bubble droplet versus the number of droplets from sample data.

This equation was fitted to the data generated in this work using Origin Pro-9.0. The Gaussian fit was achieved using Amplitude A, mean particle diameter x_C and the full width of the peak at half height (FWHM) w. An example is given in Fig. 10, where the red line is the Gaussian curve, and the Gaussian model is shown to fit the data reasonably well (see Table 1).
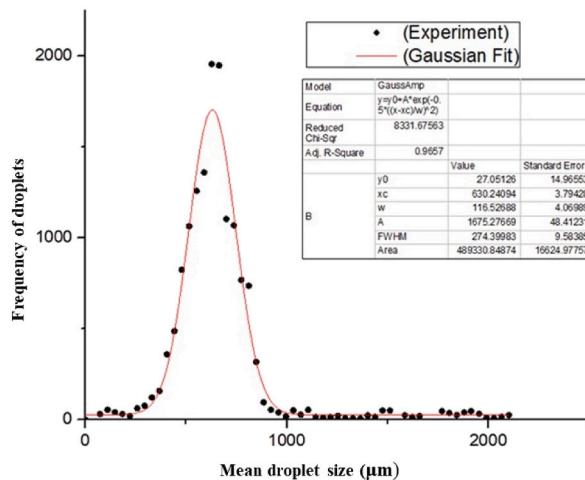

Fig. 10. Gaussian fit and experimental results.

4. Experimental results

4.1. Introduction

For practical reasons, it was decided to set up the experiment initially for equal flows in m³/h of water and oil. Four different flow rates and four different oil pad thicknesses were set. The data collected for this group of experiments was recorded in Table 2. The Theoretical understanding of how droplet properties are affected by flow and layer thickness is limited from this initial data set. It was then decided to use a statistical design of experiments to increase the number of data points and, therefore, the statistical tests that could be carried out. Minitab statistical software was used to set the experiments required. The Taguchi method was used to determine the minimum number of experiments needed to statistically investigate the effect of water flow, oil flow, and layer thickness upon droplet number, size, and distribution. The additional experiments are detailed in Table 3.

4.1.1. Visual analysis of photos

Fig. 11 (A, B, C and D) shows images of a high-speed camera for increased liquid total flow. The photos clearly show that at lower flow rates, a clear view of larger bubble droplets figure (A, B, and C) is achieved; however, as the flow rate increases, the bubble size becomes smaller (see Fig. 11 D), and the droplets become less distinct. The images for the different flow rates were then analyzed using the procedures outlined in section 3.4.

4.1.2. Gaussian fits of the dataset

Initial analysis of the experimental results was carried out for the experimental data measured for the conditions described in Table 2, where oil: water flows were maintained as 50:50 mixtures. Fig. 12 (A, B, C and D) Shows the number of droplets (Frequency) plotted as a function of the mean droplet diameter for the four oil flow rates for each layer thickness. These data points are shown fitted with simple Gaussian curves as shown in Fig. 12 (A, B, C and D).

These graphs Fig. 12 (A, B, C and D) show an inverse relationship between droplet mean diameter and bulk flow where the droplet mean diameter decreases as the bulk flow increases. On the contrary, the mean droplet diameter size increases with increase in oil pad thickness, particularly for the 36 mm thick pad. Equally, as the layer thickness increases, the spread of the peaks increases, showing an increase in the particle size range. This is believed to be caused by the droplets' increasing ability to coalesce as they pass through the oil pad.

4.2. Analysis of the Taguchi data set

The full Taguchi data set (Tables 2 and 3) were processed using Minitab to analyse the data more quantitively. Independent variables were set as oil flow, water flow, and pad thickness. The dependent variables were selected as droplet diameter, droplet frequency (Amplitude), and droplet size distribution (standard deviation). The mean of means values was calculated for each dependent variable. Graphs were plotted for each dependent variable against the independent variables to look at the separate effects of each independent variable see Fig. 13.

4.2.1. Simple plots of a mean of means droplet size against independent variables

The main effects of plots for the mean for oil, water flow rates, and oil pad thickness are shown in Fig. 13, respectively. The droplet size is strongly affected by the oil flow and responds inversely. It indicates that the mean bubble droplets decrease linearly with increasing oil flow rates. The water flow rate has a negligible impact on the droplet size and can be considered independent. Oil pad thickness shows a slight positive effect (one order of magnitude less than that seen for oil flow) on the droplet size achieved.

4.2.2. Simple plots of a mean of means amplitude (droplet frequency) against independent variables

The main effects of plots for the mean for oil, water flow rates, and oil pad thickness are shown in Fig. 14. The Amplitude (number of droplets) seems to increase enormously with both the water and oil flow rates, but conversely, it appears to decrease with increasing layer thickness. This is consistent with increased shear and turbulence due to higher flow casing and greater dispersion of the fluids. The layer works in the opposite direction because the greater residence time of the inlet flow as it passes through the oil layer in the

Table 1
Experimental results of Ballotine and Alumina oxide using image j and calliper measurements.

Ballotine			Alumina oxide		
calliper measurement	Image J measurement	percentage error	calliper measurement	Image J measurement	percentage error
mm	mm	%	mm	mm	%
1.76	1.776	−0.9%	2.1	2.109	−0.4%
1.97	1.980	−0.5%	2.17	2.184	−0.6%
2.01	2.019	−0.5%	2.29	2.293	−0.2%
2.04	2.055	−0.8%	2.32	2.322	−0.1%
2.05	2.066	−0.8%	2.46	2.466	−0.3%
2.07	2.070	0.0%	2.47	2.477	−0.3%

Table 2
Initial experimental data set for the 50:50 oil water: mixtures used to investigate the affect of oil, water flows, and layer thickness on droplet size.

Nominal water flow	Actual oil flow	Total flow	Oil Pad Thickness (mm)
m³/h			
0.227	0.227	0.454	9
			18
			27
			36
0.340	0.340	0.680	9
			18
			27
			36
0.454	0.454	0.908	9
			18
			27
			36
0.567	0.567	1.135	9
			18
			27
			36

Table 3
Additional data points measured at unequal oil-water ratios to complete the Taguchi dataset derived from the DOE.

Oil flow rate	Water flow rate	Oil pad Thickness
m³/h		mm
0.227	0.227	9
0.227	0.34	18
0.227	0.454	27
0.227	0.567	36
0.34	0.227	18
0.34	0.34	9
0.34	0.454	36
0.34	0.567	27
0.454	0.227	27
0.454	0.34	36
0.454	0.454	9
0.454	0.567	18
0.567	0.227	36
0.567	0.34	27
0.567	0.454	18
0.567	0.567	9

tank allows for more coalescence of the droplets.

4.2.3. Simple plots of a mean of means standard deviation (range of droplet sizes) against independent variables

The main effects of plots for the mean for oil, water flow rates, and oil pad thickness are shown in Fig. 15. The standard deviations, which measure the range of droplet sizes, are seen to decrease with oil flow and increase with layer thickness but are independent of water flow. The water flow result was initially considered a surprise. The water is the continuous phase, and the force it exerts on the drop is generally considered to be the main cause for the oil to shear into smaller drops. This phenomenon was observed by Ref. [26], who examined water–kerosene mixtures in a pipe over a wide range of kerosene-water compositions (zero to 50% kerosene) and flows (laminar to turbulent). Flows changes in this study barely exceed laminar flow (see Fig. 19). Compared to the work of [26], this range would be too small to see a significant effect. The oil fraction change is much more comparable with that of [26], and the increase in the range of drop sizes is consistent with their work. It is not possible with the existing apparatus to extend the range of the study to
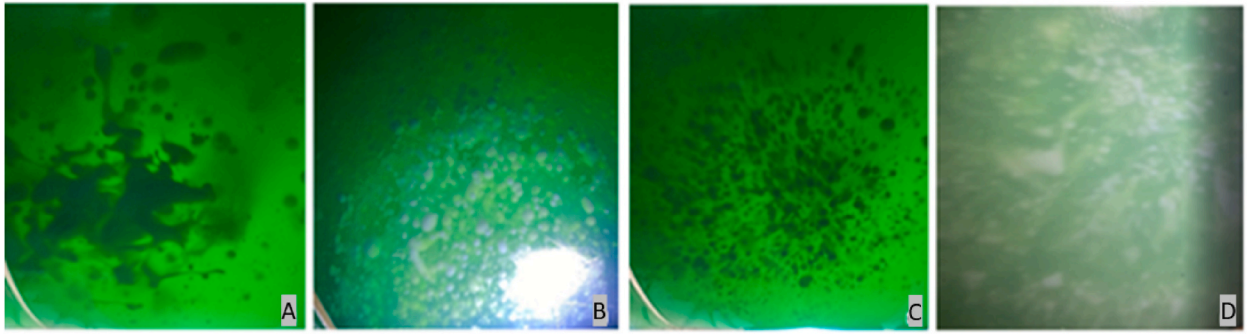
Fig. 11. Images of oil-water at different flow rates (A:0.454 m^3/h, B:0.680 m^3/h, C:0.908 m^3/h, and D:1.135 m^3/h).
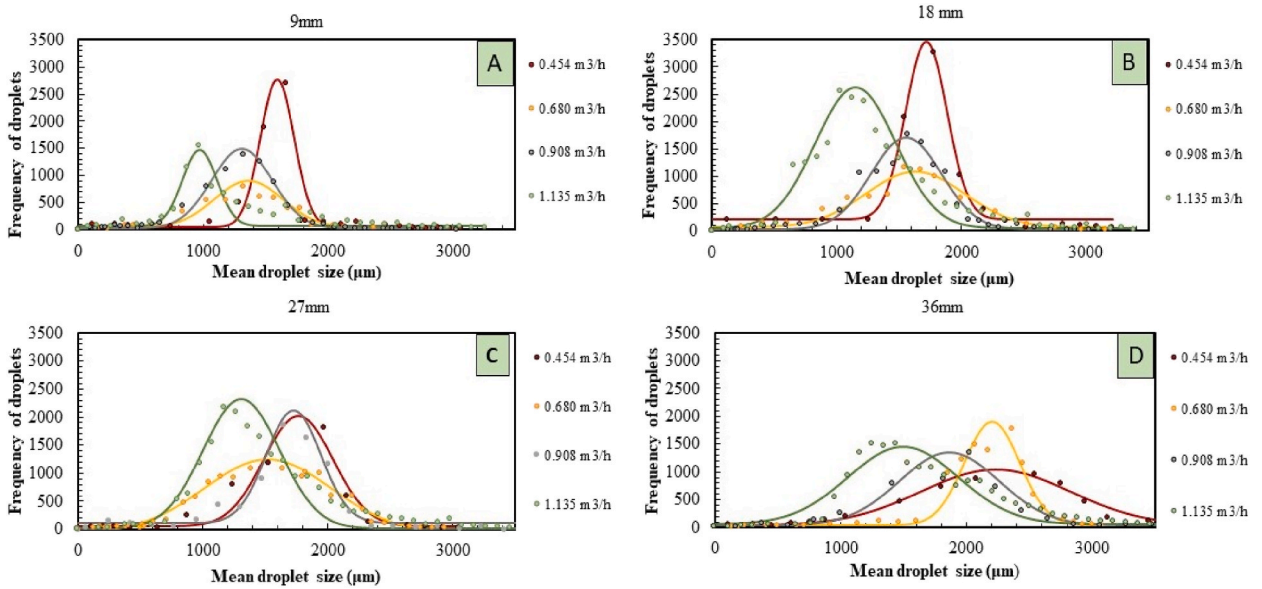

Fig. 12. Plot of the number of bubble droplets against mean droplet sizes for different oil pad thickness (A: 9, B: 18, C:27 and D:36 mm).

investigate the drop size distribution to more turbulent conditions. Equally, it is perhaps not relevant given the critical droplet sizes are those observed below the oil layer in the separator and not in the inlet pipe. In conclusion, the oil fraction and effective oil layer thickness are the significant factors that set the droplet distribution, not the overall flow regime.

4.3. Signal-to-noise ratio for three variables

The signal-to-noise ratio (SIN) measures the independent variable's effect upon the measurement relative to the noise created in the measurement from undefined sources.

For droplet size and Amplitude (Frequency) as independent variables, maximising the effect on the measurement is desirable because higher droplet frequency produces better outcomes. A higher-the-better characteristic value is one that never takes on negative values and whose highest ideal value is infinity [27]. The s/n equation (8) for this response is

$$\frac{s}{n} = -10log10\left(\frac{sum\left(1/y^2\right)}{n}\right) \tag{8}$$

It is desirable to minimise the droplet size distribution, I.e., the standard deviations, as this will reduce the number of droplets unable to settle. This is achieved by setting a lower-the-better S/N (see equation (9)). The low-the-better function cannot go below zero and does not take on negative values [27].

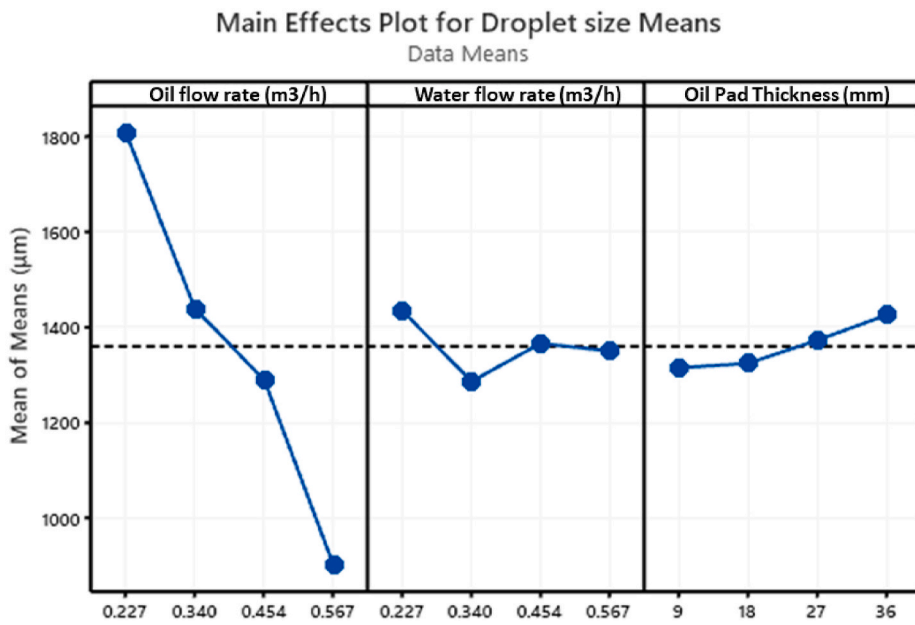$$\frac{s}{n} = -10log10\left(\frac{sum(y^2)}{n}\right) \tag{9}$$

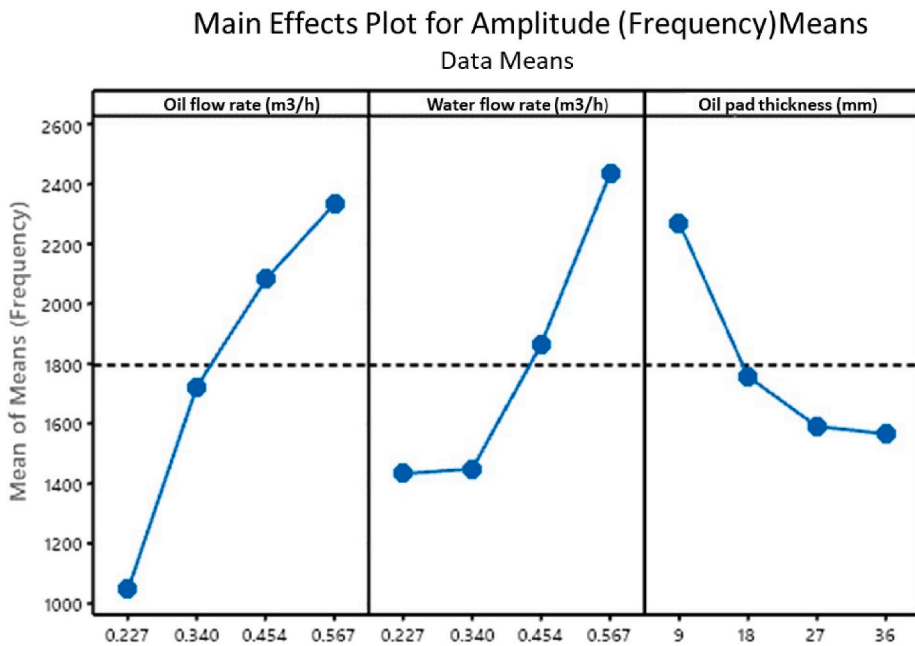**Fig. 13.** Mean of a mean plot for droplet size versus independent variables.

Fig. 14. Mean of a mean plot for Amplitude versus independent variables.

Where n is the number of experiments and y is a measured value

4.3.1. Signal-to-noise ratio for droplet size

The signal-to-noise values based on a dependent variable of droplet size are given in Table 4. The deltas values are calculated as the difference between the highest and lowest s/n ratio for a given independent variable and ranked in decreasing size. This shows that effect of the noise is minimised by varying the oil flow rate.

4.3.2. Signal-to-noise ratio for amplitude/frequency of drops

The signal-to-noise values based on a dependent variable of Amplitude are given in Table 5. This shows a similar result to the
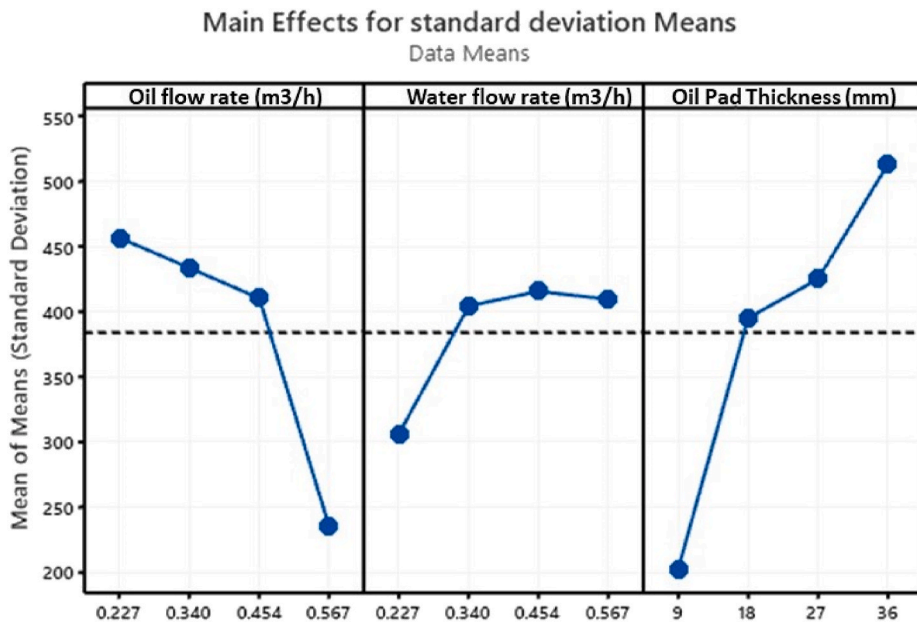
Fig. 15. Mean of a mean plot for standard deviation versus independent variables.

Table 4
Signal-to-noise values for an independent variable of droplet size.

Level	Oil flow rate	Water flow rate	Thickness
1	65.13	63.08	62.22
2	63.15	61.55	62.00
3	62.20	62.25	62.04
4	58.79	62.39	63.01
Delta	6.34	1.53	1.02
Rank	1	2	3

droplet size in that the effect of the noise is minimised by varying the oil flow rate though the effect is much reduced.

4.3.3. Signal-to-noise ratio for standard deviation (spread of droplet distribution)

The signal-to-noise values based on a dependent variable of standard deviation are given in Table 6. In this case, the oil pad thickness act most significantly to minimise the effect of noise on the measured signal.

4.4. Interaction plots of each dependent variable against the independent variables

The second stage of analysis involved plotting interaction graphs for each dependent variable. In each case, the dependent variable was plotted on the Y-axis. The primary independent variable was oil layer thickness (plotted on the Y-axis). The second independent variable was chosen as oil or water flow and plotted as separate data sets. The first set of interaction plots was produced for the droplet size and is recorded in Fig. 16.

Fig. 16 shows the lines are virtually parallel for oil flow, indicating no interactions between oil flow and oil pad thickness. Still, strong interactions are seen between water flow and oil pad thickness.

A significant impact is detected regarding the major effects of oil flow because the oil flows increase systematically for each oil pad

Table 5
Signal-to-noise values for an independent variable of Amplitude/Frequency.

Level	Oil flow rate	Water flow rate	Thickness
1	60.17	67.19	66.40
2	64.44	64.18	63.80
3	66.20	62.90	63.85
4	66.21	62.75	62.97
Delta	6.04	4.44	3.43
Rank	1	2	3

Table 6
Signal-to-noise values for an independent variable of standard deviation.

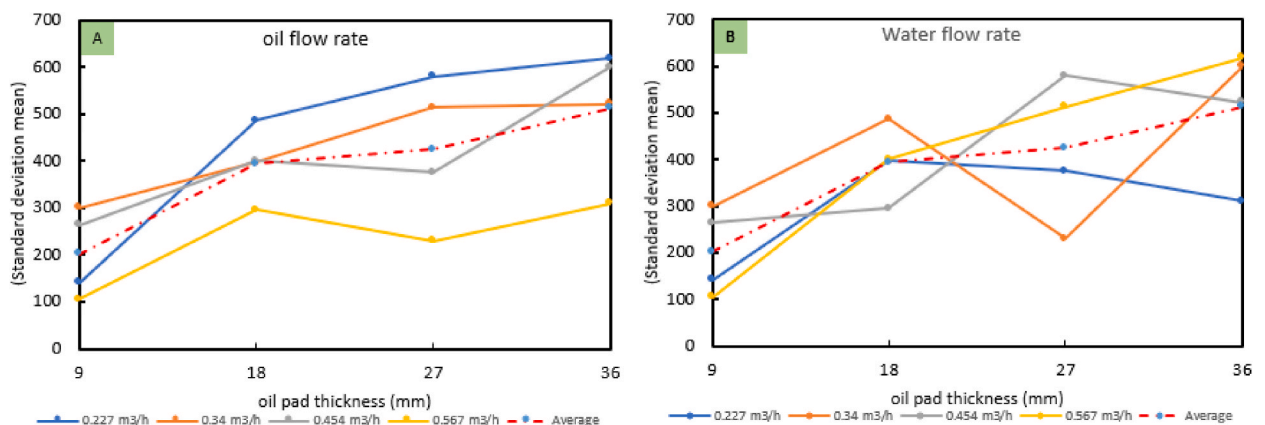| Level	Oil flow rate	Water flow rate	Thickness
1	−51.96	−49.08	−45.36
2	−52.52	−51.52	−51.80
3	−51.89	−51.87	−52.05
4	−46.73	−50.63	−53.89
Delta	5.79	2.79	8.53
Rank	2	3	1
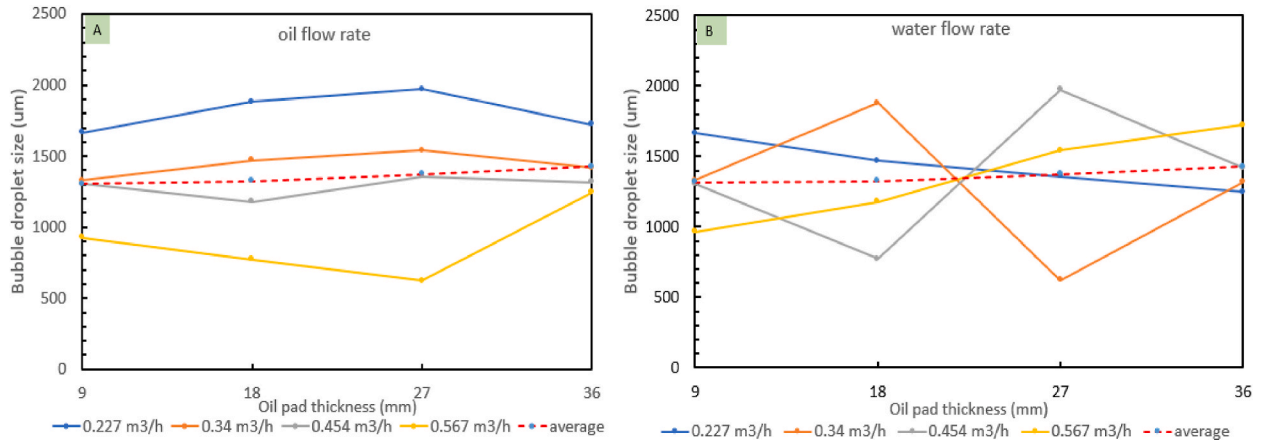
Fig. 16. Interaction of mean droplet size for oil flow rate, water flow rate, and oil pad thickness.

thickness. A second main effect is detected for the oil layer thickness with both oil and water flows because the mean droplet size for each layer thickness (shown in Fig. 16a and b) as the red dashed line) is linear and rising slightly. These results are consistent with the individual plots in Fig. 13.

(Fig. 17) shows the interaction plot for standard deviation, which measures the droplet distribution's spread. For layer thickness in the plots for water flow rate (Fig. 17B) and oil flow rate (Fig. 17A), the mean line (red dashes) rises linearly, indicating the main effect. The lines are not parallel for each independent variable, indicating an interaction between flows and oil pad thickness resulting in different droplet distributions. In terms of major effects, no major effects are seen for oil flow or water flow.

(Fig. 18A and B) shows the interaction plot for Amplitude, a measure of total droplets produced. The lines are not parallel for each independent variable, indicating an interaction between both oil and water flows and oil pad thickness resulting in different amplitudes.

In terms of major effects, no major effects are seen for any of the independent variables.

Fig. 17. Interaction of standard deviation for (A) oil flow rate against oil pad thickness, (B)water flow rate against oil pad thickness.
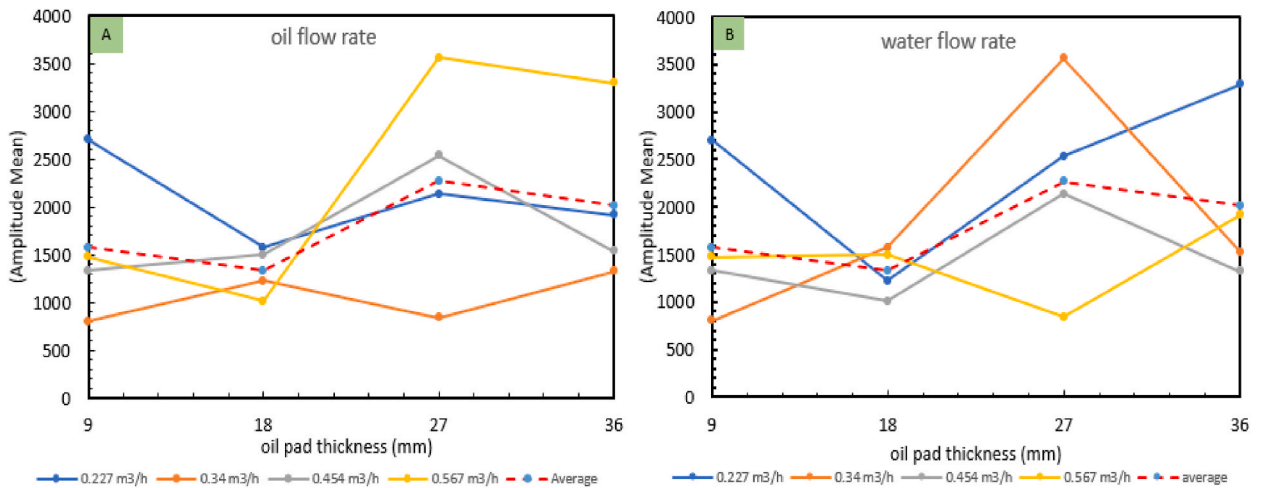
Fig. 18. Interaction of Amplitude for (A) oil flow rate against oil pad thickness, (B) water flow rate against oil pad thickness.
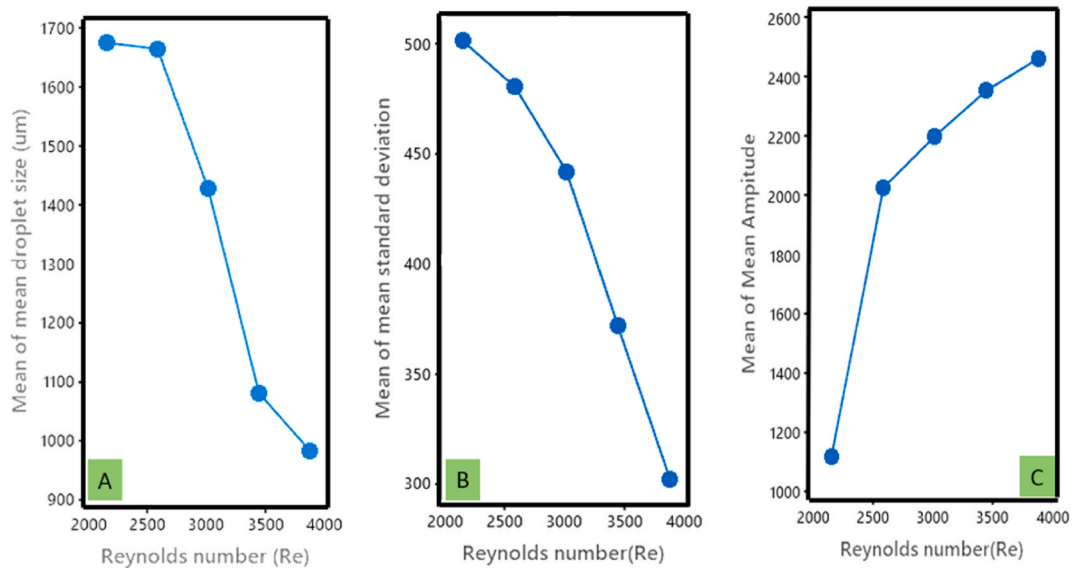

Fig. 19. Reynolds number against (A) droplet size, (B) standard deviation, and (C) Amplitude.

4.4.1. Overall conclusions for Taguchi analysis

The Taguchi analysis of the data has shown for droplet size that:

1) Oil flow rate is the dominant parameter controlling droplet size.
2) Oil pad thickness has some effect on droplet size, but no interaction is seen between oil flow rate and layer thickness.

For the spread of the droplet sizes (standard deviation)

1) There are interactions between both flows and oil pad thickness in different droplet distributions that would be achieved if either variable changed on its own.
2) The main effect is detected for the layer thickness, where the spread is seen to rise with thickness.

For the number of droplets produced (Amplitude)

1) The number of droplets increases with both oil and water flow rates but decreases with oil pad thickness. There are clear interactions between all variables resulting in different droplet frequencies for the combined effects.

4.5. Analysis based upon inlet pipe Reynolds number

The analysis so far has related to droplet size distribution in the vessel and has looked at truly independent variables based on the separate flows of oil and water. However, in practice, the feed enters as a fully mixed stream and could be considered as such. The Reynold number is a way of accounting for the mixed properties of the stream and could be considered an independent variable see Fig. 19 (A, B and C). There is insufficient data to do a full Taguchi analysis, but it is possible to compare the mean of means trends for each independent variable against the dependent variables.

4.5.1. Overall conclusions for Reynolds numbers (R_e)
The analysis of the Reynolds number data has shown that:

1) Adjusting the Reynolds number in a system can control the mean droplet size. The mean droplet size decreases linearly as the Reynolds number increases. This suggests that the Reynolds number may be a crucial factor when designing droplet-based systems, as it can be used to control droplet size. Additional research may be required to understand the relationship between the Reynolds number and droplet size and determine the best methods for adjusting the Reynolds number to achieve the desired droplet size.
2) The standard deviations of droplet sizes decreased as the Reynolds numbers increased. This indicates that as the Reynolds numbers increased, the range of droplet sizes became narrower.
3) It was observed that the number of droplets increased as the Reynolds number increased. This suggests that higher Reynolds numbers lead to a greater number of droplets being produced.

5. Conclusions

In this study, simple image capture measurement techniques were developed and applied to record bubble size distributions of water in oil droplets created in a two-phase separator. The experiments were conducted using a transparent laboratory separator, and the DOE method with Taguchi analysis was applied to analyse the results. The resulting data was used to examine the different parameters that could affect droplet sizes. The findings showed that droplet properties could be modelled using Gaussian distributions.

Statistical analysis indicated that droplet size is influenced by both the oil flow rate and oil pad thickness. The oil flow rate was found to have the most significant impact on droplet size, while the effect of oil pad thickness was minor. No interaction was found between these two parameters.

For the number of droplets produced the effects are complex: the number of droplets increases with both oil and water flow rates but decreases with oil pad thickness. There are clear interactions between all variables resulting in different droplet frequencies for the combined effects.

For the distribution of the droplet sizes: the main effect is detected for the layer thickness, where the spread is seen to rise with thickness. However, there are interactions between both flows and oil pad thickness and different droplet distributions would be achieved if either variable changed on its own.

Author contributions

Kul pun: Conceived and designed the experiments; Performed the experiments; Analyzed and interpreted the data; Contributed reagents, materials, analysis tools or data; Wrote the paper.

Faik Hamad: Conceived and designed the experiments; Wrote the paper.

Tariq Galadanchi Ahmad: Conceived and designed the experiments; Analyzed and interpreted the data; Wrote the paper.

Johnson Ugwu, Safa Amir Najim: Analyzed and interpreted the data.

James Eyers: Analyzed and interpreted the data; Contributed reagents, materials, analysis tools or data.

Gary Lawson Conceived and designed the experiments; Contributed reagents, materials, analysis tools or data.

Paul A. Russell: Conceived and designed the experiments; Performed the experiments; Analyzed and interpreted the data; Wrote the paper.

Declaration of competing interest

The authors state that they have no financial or personal affiliations that might have influenced the work presented in this publication.

Funding

Data availability statement

Data will be made available on request.

Acknowledgements

References

[1] H. van Asselt, Breaking a Taboo: Fossil Fuels at COP26, Breaking a Taboo: Fossil Fuels at COP26 – EJIL: Talk!, 2021. Available at: www.ejiltalk.org. (Accessed 5 April 2022) https://www.ejiltalk.org/breaking-a-taboo-fossil-fuels-at-cop26/. Accessed.

[2] Short-Term Energy Outlook, Washington, D.C: Energy Information Administration, Office Of Energy Markets And End Use, U.S. Dept. Of Energy, 2022. Available at: https://www.eia.gov/outlooks/steo/report/global_oil.php. (Accessed 6 April 2022). Accessed.

[3] L. Wood, Global Three-phase Separator Market in the Oil and Gas Industry 2018-2022 - ResearchAndMarkets, 2018 com Available at: https://www.businesswire.com/news/home/20180807005429/en/Global-Three-phase-Separator-Market-in-the-Oil-and-Gas-Industry-2018-2022-ResearchAndMarkets.com. (Accessed 5 April 2022). Accessed.

[4] T.G. Ahmed, Optimisation of Three-phase Separator Design through Computational Fluid Dynamics Simulation and Experimental Investigation, Teesside University, 2021.

[5] W. Monnery, W. Svrcek, Successfully specify three-phase separators, Chem. Eng. Prog. 90 (9) (1994) 29–40.

[6] M. Stewart, K.E. Arnold, Surface production operations, in: Design of Oil Handling Systems and Facilities, ume 1, 2008.

[7] N. Kharoua, L. Khezzar, H. Saadawi, Using CFD to Model the Performance of Retrofit Production Separators in Abu Dhabi', Society of Petroleum Engineers - Abu Dhabi International Petroleum Exhibition and Conference 2012, ADIPEC 2012 - Sustainable Energy Growth: People, Responsibility, and Innovation, vol. 3, 2012, pp. 1776–1784, https://doi.org/10.2118/161521-ms.

[8] c. c. Wright, D.w. Douglas, The Disposal of APA Oil Field Wastewater, American petroleum institute, 1966.

[9] w. b. Hopper, l. jacobs, Handbook of Separation Techniques for Chemical Engineers, 3 ed., 1996 (s.l.:s.n).

[10] A. Pourahmadi Laleh, CFD Simulation of Multiphase Separators, University of Calgary-doctoral thesis, Calgary, 2010.

[11] M. Walas, Stanley, Chemical Process, Equipment Selection and Design, USA inc, USA, 1990.

[12] L.M. Oshinowo, R.D. Vilagines, Modeling of oil-water separation efficiency in three-phase separators: effect of emulsion rheology and droplet size distribution, Chem. Eng. Res. Des. 159 (2020) 278–290, https://doi.org/10.1016/j.cherd.2020.02.022.

[13] Z. Khalifat, M. Zivdar, R. Rahimi, Simulation of an Industrial Three Phase Boot Separator Using Computational Fluid Dynamics, 2019, pp. 30–43. April.

[14] J.H. Song, et al., Three-phases separator sizing using drop size distribution, Proceed. Ann. Offshore Techn. Conf. 2 (May) (2010) 1011–1023, https://doi.org/10.4043/20558-ms.

[15] A. Ghaffarkhah, Z.A. Dijvejin, M.A. Shahrabi, M.K. Moraveji, M. Mostofi, Coupling of CFD and semiempirical methods for designing three-phase condensate separator: case study and experimental validation, J. Pet. Explor. Prod. Technol. 9 (1) (2019) 353–382, https://doi.org/10.1007/s13202-018-0460-5.

[16] L. Oshinowo, E. Elsaadawy, R. Vilagines, Cfd Modeling Of Oil-Water Separation Efficiency In Three-Phase Separators, 2014. Available at: www.sintefbok.no.

[17] A.H. Kamel, S.A. Akashah, F.A. Leeri, M.A. Fahim, Particle size distribution in oil-water dispersions using image processing, Comput. Chem. Eng. 11 (4) (1987) 435–439.

[18] S. Narayan, D.B. Moravec, B.G. Hauser, A.J. Dallas, C.S. Dutcher, Removing water from diesel fuel: understanding the impact of droplet size on dynamic interfacial tension of water-in-fuel emulsions, Energy Fuels 32 (7) (2018) 7326–7337.

[19] D.A. Wilson, K. Pun, P.B. Ganesan, F. Hamad, Geometrical optimisation of a venturi-type microbubble generator using CFD simulation and experimental measurements, Design 5 (1) (2021) 1–18, https://doi.org/10.3390/designs5010004.

[20] L.S. Zhai, et al., Measurement of droplet sizes in bubbly oil-in-water flows using a fluid-sampling device", Measurement, J. Int. Measur. Conf. 102 (2017) 296–308, https://doi.org/10.1016/j.measurement.2017.01.055.

[21] Rishi Kumari, Narinder Rana, Particle size and shape analysis using ImageJ with customised tools for segmentation of particles, Int. J. Eng. Res. V4 (11) (2015) 247–250, https://doi.org/10.17577/ijertv4is110211.

[22] D. Laupsien, C. Le Men, A. Cockx, A. Liné, Image processing for bubble morphology characteristics in diluted bubble swarms, Phys. Fluids 31 (5) (2019), 053306, https://doi.org/10.1063/1.5088945.

[23] K. Pun, F.A. Hamad, T. Ahmed, J.O. Ugwu, J. Eyers, G. Lawson, P.A. Russell, Investigation of droplet size produced in two-phase gravity separators, Int. J. Civ. Mech. Eng. 17 (1) (2023) 6–10.

[24] T. lappalainen, J. Lehmonen, Determinations of bubble size distribution of foam-fibre mixture using circular hough transform, Nord. Pulp Pap Res. J. 27 (5) (2012) 930–939, https://doi.org/10.3183/NPPRJ-2012-27-05-p930-939.

[25] F. Guo, Y. Yang, B. Chen, L. Guo, A novel multi-scale edge detection technique based on wavelet analysis with application in multiphase flows, Powder Technol. 202 (1–3) (2010) 171–177.

[26] F.A. Hamad, M.K. Khan, H.H. Bruun, Experimental study of kerosene–water two-phase flow in a vertical pipe using hot-film and dual optical probes, Can. J. Chem. Eng. 91 (2013) 1296–1311, https://doi.org/10.1002/cjce.21743.

[27] G. Taguchi, Introduction to Quality Engineering: Designing Quality into Products and Processes, 1986.

Kul Pun holds a BSC and MSc degree in Mechanical Engineering from Teesside University. Before enrolling in a Ph.D. program, he worked as a senior researcher engineer (Multiphase flows, microbubble generation, and flow in porous media and microchannels) at Teesside University School of Computing, Engineering, and Digital Technology. A Ph.D. candidate is designing a three-phase separator for teaching and research purposes using CFD and experimental work at Teesside University and the R & D Engineer at the Darbytech Engineering Wilton workshop.

Dr. Faik A. Hamad has been a senior lecturer in the engineering department at Teesside University's School of Computing, Engineering, and Digital Technology since 2011 and was promoted to Associate professor in 2020. He spent four years as a researcher/teaching fellow at Aberdeen University before joining Teesside University. Hamad has co-authored over 70+ articles in prestigious journals and as a reviewer for several others. His research interests are multiphase flows, energy storage, microbubble technology, filtration, aerodynamics, and turbomachinery. Hamad recently received six grants that will allow him to expand his research into new areas such as microbubble generation, multiphase flow in pumps and high-temperature heat pipe exchangers for nuclear applications.

Dr. Tariq G. Ahmed is a Lecturer in Engineering at the School of Computing Engineering and Digital Technologies. He holds the Chartered Engineer (C.Eng) status with the Institute of Materials Minerals and Mining and is also a member of the Energy Institute (E.I.) and Society of Petroleum Engineering (SPE). Tariq completed his BEng (Hons) in Chemistry from Kano University of Science and Technology Wudil, MSc in Petroleum Engineering, and a Ph.D. in Separator Optimisation from Teesside University. His research is mainly focused on Separator optimisation, CFD modelling of surface separation equipment, and Hydrogen Fuel.

Dr. Johnson Ugwu, **Ugwu** is a Senior Lecturer in Energy and Environmental Engineering at Teesside University's School of Computing, Engineering, and Digital Technologies. He is a Chartered Energy & Petroleum Engineer and a fellow of the higher education academy (FHEA). His teaching and research interests include the following. Pilot plant and bio-refinery designs, Process design and simulation for Net-Zero Technologies, in-situ hydrogen production from natural gas reservoirs, Energy mix evaluation, and optimisation of energy transition routes for the hydrogen economy. Oil and Gas field development planning, Production Optimisation and Management Benchmarking petroleum fluid property models using Machine learning algorithms, Multiphase flow in porous and permeable media, Classical and Numerical Reservoir modelling and Simulation, IOR/ EOR, drilling engineering and safety management.

Dr. Najim A. Safa has been a professor at Basrah University's Electrical Engineering Department since 2016. In 1973, he was born in Basrah, Iraq. He achieved his PhD from Bangor University in the United Kingdom. His study has focused on software engineering for visualising complex data sets, such as those from medical imaging and remote sensing imagery. His areas of study include neural networks, image analysis, emotion, and parallel processing in graphics processing units GPU.

James Eyers holds a First-Class master's degree in chemical engineering and is an Associate Member of the Institution of Chemical Engineers (AMIChemE). He is a Prototype Design Engineer at DarbyTech and is currently focused on the development of a computer-controlled, lab-scale teaching/research rig demonstrating the production and use of hydrogen.

Gary Lawson holds an Honours Degree in Electrical and Electronic Engineering, is a Chartered Electrical Engineer, and is a Fellow of the Institute of Engineering & Technology. Following graduation as a sponsored student with British Steel, he followed a career with British Steel. He then joined a multi-disciplined engineering, manufacturing, and construction contracting organisation, becoming Director of a portfolio of businesses in the U.K. and overseas. He has over 30 years of experience delivering projects across most industrial sectors, has been chair of the Teesside branch of the IET, and has been involved with designing and supplying industrial training equipment for education for the last ten years.

Dr. Paul A. Russell is a senior lecturer in chemical engineering at Teesside University's School of Computing, Engineering, and Digital Technologies. His scientific interests are optimising three-phase separators, monitoring small flows with flux-response technology, gas adsorption, distillation, and experimental studies of heterogeneously catalysed processes in microreactors.